J Mater Sci: Mater Electron **(2024) 35:1268**

Sensing volatile organic compounds with CVD graphene: insights from quartz crystal microbalance and surface plasmon resonance studies

Hakan Selvi[1], Inci Capan[2], Rifat Capan[2], and Yaser Acikbas[1,*]

[1] *Department of Materials Science and Nanotechnology Engineering, University of Usak, 64200 Usak, Turkey*
[2] *Department of Physics, Faculty of Science, University of Balikesir, 10145 Balikesir, Turkey*

Received: 18 February 2024
Accepted: 23 June 2024
Published online: 28 June 2024

ABSTRACT

This study explores the sensing capabilities of chemical vapor deposition (CVD)-grown graphene in detecting volatile organic compounds (VOCs) through quartz crystal microbalance (QCM) and surface plasmon resonance (SPR) techniques. Two distinct sensing devices were developed, each tailored for QCM and SPR transducing mechanisms, utilizing CVD graphene as the sensing element. The sensors demonstrated consistent and reproducible responses when exposed to various concentrations of dichloromethane, chloroform, carbon tetrachloride, benzene, toluene, and m-xylene. Notably, both sensors exhibited unparalleled sensitivity to dichloromethane, with the graphene-coated SPR sensor displaying a sensitivity value of 294×10^{-3} ppm^{-1} and a limit of detection (LOD) value of 10.62 ppm. Additionally, the SPR sensor showcased remarkably swift response and recovery times, both under 3 sec. Results indicate that the adsorption of VOC molecules on the CVD graphene surface increases with the rising dipole moments and vapor pressure values of the molecules. The utilization of CVD graphene in both sensing approaches demonstrates good reproducibility in detecting ultralow concentrations of VOCs at room temperature.

1 Introduction

The increase in volatile organic compounds (VOCs) emissions in recent years has raised concerns about their impact on human health and air quality [1]. Several VOCs have been identified as highly hazardous or carcinogenic and can have both short-term and long-term effects on human health and the environment [2, 3]. To address these issues, organizations such as the World Health Organization and the Environmental Protection Agency have issued guidelines to limit the concentration of VOCs in indoor and workplace environments [4].

In environmental monitoring, VOC sensors are employed for various purposes, including monitoring indoor air quality [5], controlling traffic emissions [6], and regulating industrial emissions and pollution [7]. However, the utility of VOC sensing extends far beyond environmental concerns, encompassing a diverse range of fields. In healthcare, VOC sensing is

Address correspondence to E-mail: yaser.acikbas@usak.edu.tr

https://doi.org/10.1007/s10854-024-13087-1

indispensable for disease detection and human body monitoring [8]. Certain VOCs found in human biological fluids like blood, breath, sweat, and urine act as biomarkers for various health conditions such as detecting mental disorders [9], infectious diseases [10], and cancer [11]. Similarly, in food security, VOC sensing plays a crucial role in evaluating food quality and safety [12]. VOC sensors can detect specific variations in VOC concentrations and types indicating spoilage, either through the alteration of existing VOC concentrations or the introduction of new VOCs due to bacterial oxidation [13].

In the field of VOCs analysis, two primary methodologies are frequently employed. The first approach utilizes analytical techniques such as gas chromatography mass spectrometry (GC–MS) [14, 15], while the second approach utilizes solid-state sensors, including those based on metal oxide semiconductors (MOS) [14, 16, 17], electrochemical (EC) methods [18, 19], and photoionization detection (PID) [20, 21]. While GC–MS can produce precise analysis of gases, the equipment required for this method is large and therefore not well-suited for point-of-use or real-time applications. In contrast, solid-state chemical sensors offer high sensitivity and portability, but possess limited selectivity to distinguish among various VOCs [22]. To address this limitation, alternative transducing principles such as capacitive [23], electrochemical [18, 24], surface acoustic wave [25], optical [26, 27], and gravimetric [28] have been explored for VOC detection utilizing a variety of materials, including semiconducting metal oxides [8], carbon-based nanomaterials [29], and nanocomposites [30–32].

The discovery of graphene has opened up unprecedented opportunities across various domains, spanning from optoelectronics to biomedicine [33]. Graphene exhibits remarkable mechanical, electronic, and optical properties, deriving from its perfect two-dimensional sp2-bonded structure [33–35]. These properties enable a wide range of applications, including next-generation flexible electronics [36], photovoltaics [37], filtration systems [38], energy storage technologies [39], and tissue engineering, highlighting its versatility and potential impact across scientific disciplines.

One of the most promising avenues lies in utilizing graphene for realizing ultrafast and ultrasensitive sensor applications [40, 41]. Graphene possesses the greatest surface area per unit volume, with every carbon atom in graphene acting as a surface atom. Consequently, when a chemical species interacts with graphene, it alters the structure and electronic system of graphene in its native state.

This modification can be used to detect an interaction or binding event. Additionally, graphene has intrinsically low electrical noise owing to its high mobility and unique crystal lattice, so even the exchange of a few electrons as a result of an interaction can cause a detectable shift in the carrier concentration [42]. Because of these properties, graphene is an excellent candidate for ultrasensitive gas detection in a variety of settings; in fact, single-molecule detection with graphene has been successfully demonstrated by measuring the resulting change in Hall resistivity at cryogenic temperatures [42]. Graphene's large surface area and π-electron system contribute to its pronounced affinity for VOCs. The presence of defect sites with dangling bonds and functional groups can further enhance this affinity. The interaction between graphene and VOCs can arise from hydrogen bonding, Van der Waals forces due to possible induced dipoles, and charge transfer [43, 44]. These mechanisms collectively influence graphene's suitability for detecting VOCs in various environments.

Presently, commercially available gas sensors utilizing metal oxide materials have been optimized for detecting volatile organic compounds (VOCs) at parts per million (ppm) levels [30]. However, these sensors suffer from drawbacks including slow response times, lack of selectivity, and a need for high operating temperatures above 200 °C. In contrast, graphene demonstrates sensitivity to NH_3 [45] and NO_2 [46] even at ambient room temperature, with concentrations down to the range of parts per million (ppm) levels. Furthermore, advancements in graphene-based gas sensors have enhanced selectivity through functionalization with aromatic molecules, polymers, and metal nanoparticles [47].

In the present work, we integrate chemical vapor deposition (CVD) graphene onto suitable substrates with conventional QCM and SPR sensing approaches for the first time to investigate the sensing performance of graphene against VOCs in two separate sensing modalities. Our results showed that CVD graphene has highly sensitive and selective responses to dichloromethane vapor than others.

2 Experimental details

2.1 Sensor preparation

Commercially supplied graphene produced by CVD technique on copper was employed to fabricate two sets of sensors: a graphene-coated QCM sensor deposited onto a QCM crystal and a graphene-coated SPR sensor deposited onto a 50-nm-thick gold-coated glass substrate. The flow of the experimental process is depicted in Fig. 1. The fabrication process starts with spin coating a support layer of poly-methyl-methacrylate (PMMA) with a molecular weight of 950 k, dissolved in a 4% anisole solution, onto a monolayer CVD graphene film on copper foil. This PMMA support layer enables the transfer of graphene film from the copper foil to the desired substrates. To minimize the potential damage caused by centrifugal force on graphene, the rotation speed was gradually increased from 750 to 2500 rpm. Consequently, this process led to the deposition of a PMMA layer approximately 300 nm in thickness. The graphene coating on the reverse side of the foils was then removed using a mild O_2/Ar plasma etch.

Next, the copper foil with the support layer was floated on a solution of ammonium persulfate (20 g/L), which etches away the copper foil, releasing the graphene adhered to the support layer. The floating graphene/PMMA membrane was scooped onto a Si/SiO_2 substrate and quickly redeposited on a water surface for rinsing to remove any copper and etchant residues. The membrane was then scooped out onto the final substrate (QCM or SPR) and air-dried.

The substrate with the PMMA/graphene membrane was then baked for 5 min at 130 °C to improve graphene adhesion to the substrates. Next, the PMMA film was removed from the substrates by immersing it in an acetone bath for 2 hours. Finally, the substrates were rinsed in isopropyl alcohol (IPA) and gently dried with a nitrogen gun.

Raman spectroscopy (Renishaw inVia) was performed using a 532 nm laser excitation to assess the structural and electronic properties of CVD graphene on copper foil. The shapes, intensities, and positions of the characteristic Raman peaks—D, G, and 2D bands—offer valuable insights into the graphene domains, including layer numbers and overall film quality [48]. The obtained Raman spectrum of graphene, depicted in Fig. 2, reveals a minimal D peak and a single Lorentzian 2D peak with a full width at half maximum (FWHM) below 40 cm^{-1}. This confirmation indicates that the graphene films predominantly consist of single-layer graphene with few defects, as validated by Raman spectroscopy.

Two separate sets of sensing devices, employing graphene as their primary sensing element, were manufactured and investigated for their responses when exposed to different volatile compounds. Dichloromethane, chloroform, carbon tetrachloride, benzene, toluene, and m-xylene at varying concentrations were

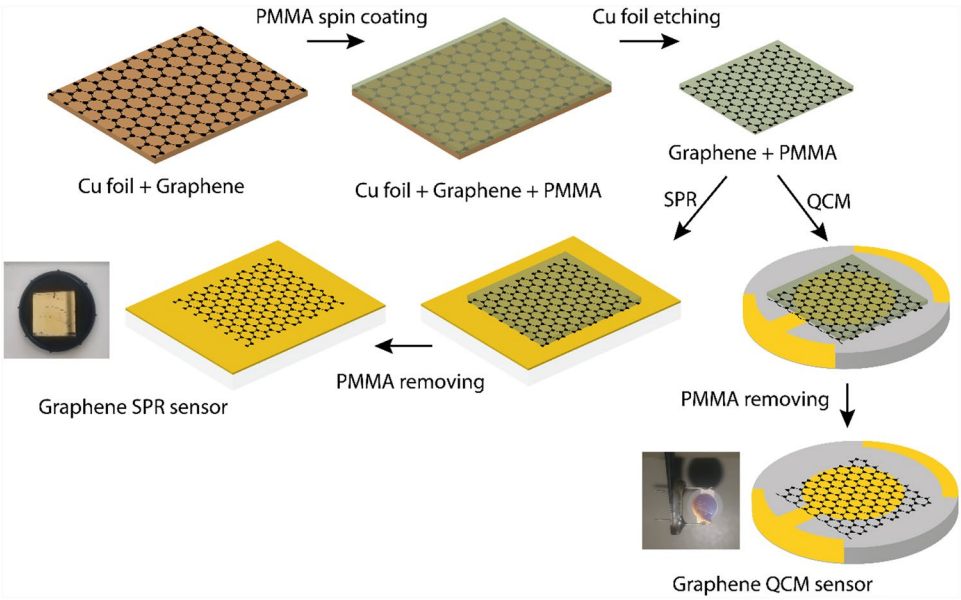

Fig. 1 Fabrication process of the graphene-coated SPR and graphene-coated QCM sensors

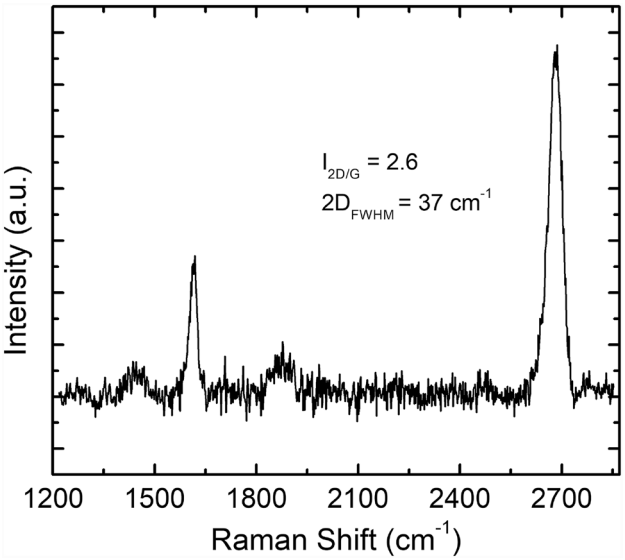

Fig. 2 Raman spectrum of the graphene film on copper foil

meticulously prepared, and these devices were subsequently examined using QCM measurement and SPR systems.

2.2 QCM measurement system

QCM sensors have been widely adopted as a portable transducer element for chemical sensors since it is highly stable, cost-effective, and enables in situ and real-time monitoring of analytes. A visual representation of a custom designed QCM kinetic measurement system is presented in Scheme 1. This system features a thinly cut quartz crystal wafer with metal-coated electrodes arranged in an overlapping keyhole design, resonating at a nominal frequency of 3.5 MHz. This quartz crystal is positioned within a gas cell, linked to an electronic control unit that interfaces with a PC computer. An alternating voltage, applied across the electrodes of the quartz crystal oscillator through a power supply, induces oscillations at its designated frequency.

The mass increase due to adsorption exhibits a linear correlation with the change in oscillation frequency, as determined by the well-established Sauerbrey Equation [49]. The PC computer, equipped with specialized software, records the frequency change as a function of time, constituting the real-time kinetic response. It serves as a valuable tool for exploring all interaction details between the graphene surface and VOC molecules, enabling the evaluation of the sensing capabilities of the graphene-coated QCM sensor. The testing procedure involves exposing the graphene-coated sensor to organic vapor at designated time intervals, followed by a recovery phase facilitated by the introduction of fresh air. This repetitive cycle is performed a minimum of three times to evaluate the repeatability of the graphene-coated QCM sensor.

2.3 SPR measurement system

In the SPR sensing methodology, refractive index changes play a crucial role in achieving label-free detection and real-time monitoring of molecular interactions [50]. Diverging from QCM sensing, which predominantly gauges changes in mass near the sensor

Scheme 1 QCM measurement system

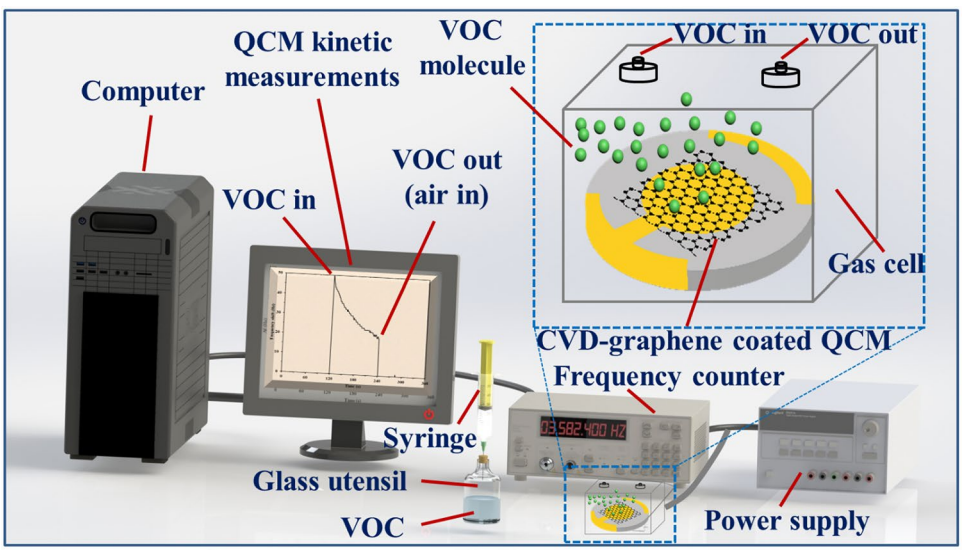

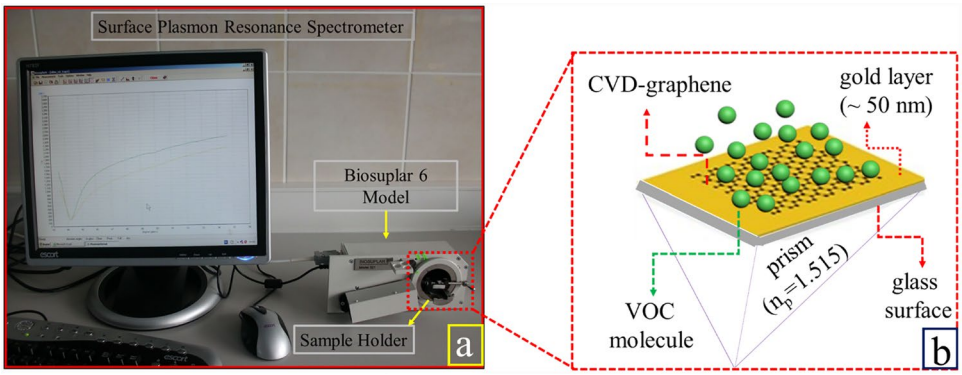

Scheme 2 **a** SPR technique, **b** Kinetic study scheme for graphene-based SPR sensor

surface, SPR excels in its sensitivity to alterations in refractive index at the interface between the sensing material and the surrounding medium [51].

To investigate the sensing performance of CVD graphene against VOC molecules in an optical transducing modality, we transferred CVD graphene onto a glass slide with a uniformly coated 50-nm-thick gold film to form a graphene SPR sensor. The interaction between CVD graphene and vapor molecules, whether through chemical binding or physical adsorption, may induce changes in the optical refractive index, promising precise measurement of low concentrations of VOCs.

Scheme 2a illustrates the configuration employed for measuring SPR responses with the Biosuplar 6 SPR spectrometer device. This setup utilized the Kretschmann geometry and featured a retro-reflecting measurement prism mounted on a rotating table.

Presented in Scheme 2b is the symbolic representation of the kinetic measurements. The sensor details involve securely attaching the glass slide's backside to the base of the prism ($n_p = 1515$) using an immersion liquid with a refractive index match. The front side of the glass slide, which features a 50 nm gold layer with CVD graphene transferred onto it, is positioned directly facing the gas cell. The CVD graphene coating was illuminated by transversely polarized light (632.8 nm) from a He–Ne laser. The variation in the intensity of reflected light at a fixed angle was monitored over time as the CVD graphene SPR sensor underwent transient exposure to VOCs of interest for 2 min. This exposure was followed by a 2-min recovery period during which fresh air was introduced into the gas cell. The tests were conducted at room temperature (20 ℃).

To examine the impact of concentration on the response of a graphene-coated SPR sensor, we subjected it to varying concentrations of dichloromethane molecule. Specifically, we prepared diluted saturated vapor mixtures with dry air at concentrations of 25%, 50%, 75%, and 100%. Throughout these exposure sequences, the intensity of reflected light changed with the introduction of VOC molecules into the gas cell. As anticipated, heightened gas concentrations correlated with an increased sensor response, aligning with predictions, and highlighting the SPR sensors' sensitivity to changes in gas composition.

3 Results and discussions

3.1 QCM and SPR kinetic measurement results

Utilizing the QCM sensor with a CVD graphene coating, we investigated the interaction kinetics between the graphene surface and various VOCs to evaluate graphene's vapor sensing capabilities. Figure 3 provides a symbolic representation of the kinetics of the interaction between the graphene film and the vapor, where the frequency shift (Δf) is recorded over time. In the initial step, we introduced fresh air into the gas cell for a duration of 120 s to establish a stable baseline resonance frequency value for our measurements. During this period, the frequency change over time remained nearly constant, indicating the attainment of a reliable baseline before the introduction of the targeted VOC molecules. Subsequently, at the 120th second, the injection of organic vapor into the gas chamber led to a rapid increase in the response of graphene-coated QCM sensors to the organic vapor (surface adsorption process).

Notably, the QCM frequency value returned to its baseline after 240 s, following the reintroduction of

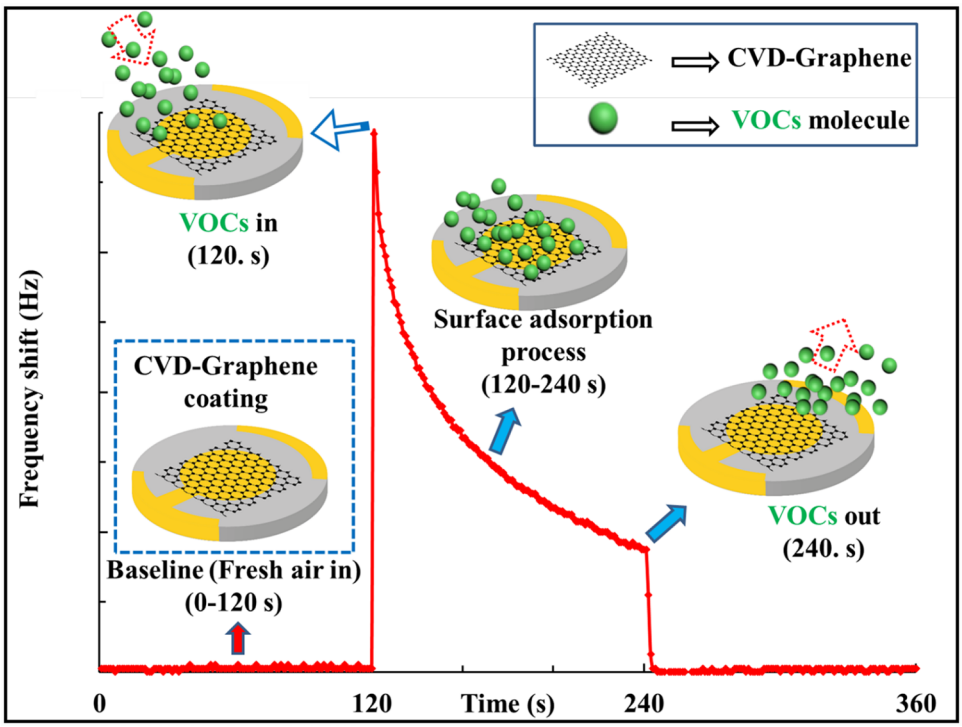

Fig. 3 A symbolic representation of the QCM-gas kinetic mechanism

fresh air molecules into the gas cell. This observation underscores the reversible response of graphene-coated QCM sensors, indicating their capacity to recover for subsequent measurements.

Our results reveal consistent response patterns exhibited by graphene-coated QCM sensors when exposed to a range of VOCs.

As depicted in Fig. 4, the interaction kinetics of the graphene-coated QCM sensor was examined in the presence of saturated concentrations of various vapors. During the initial 120 s, a stable baseline resonance frequency was consistently recorded when fresh air was introduced into the gas cell. Subsequently, a notable change in resonance frequency occurred between 120 and 240 s, coinciding with the injection of organic vapor molecules into the gas cell. This change corresponded to the surface adsorption of vapor molecules onto the graphene surface. The baseline resonance frequency was re-established upon the introduction of fresh air at the 240-s mark, indicating the sensor's reversible response to each type of vapor.

The importance of defect sites in gas sensing is well acknowledged. In its typical preparation, graphene inherently possesses oxidation defect sites and dangling bonds, distributed both along the edges and across its basal plane [52]. Commonly introduced during the synthesis or transfer process, these oxidation defects involve (C = O), (CO), (OC = O), and (OH) [53]. These defect sites engage with vapors, primarily through weak hydrogen bonding or Van der Waals interactions [54, 55].

Consequently, the observed reversible and relatively fast dynamic response in Fig. 4 suggests that vapor adsorption on graphene structure is primarily of the physical type such as Van der Waals forces, charge-transfer interactions, and the formation of hydrogen bonding through functional groups on the graphene surface such as oxygen-containing groups [55].

Notably, the graphene-QCM sensor demonstrated the highest sensitivity to dichloromethane, reflected in the frequency shift, surpassing the sensitivity to other aromatic compounds. The sensitivity order, listed in decreasing intensity, is as follows: dichloromethane > chloroform > carbon tetrachloride > benzene > toluene > m-xylene.

Dichloromethane is a molecule with a substantial dipole moment due to its polar nature. It may engage with graphene via dipole-induced dipole interactions. This significant dipole moment enhances its adsorption on the graphene surface. The order of dipole moments of the tested VOCs from highest to lowest is as follows: dichloromethane > chloroform > benzene ≈ toluene ≈ m-xylene > carbon tetrachloride.

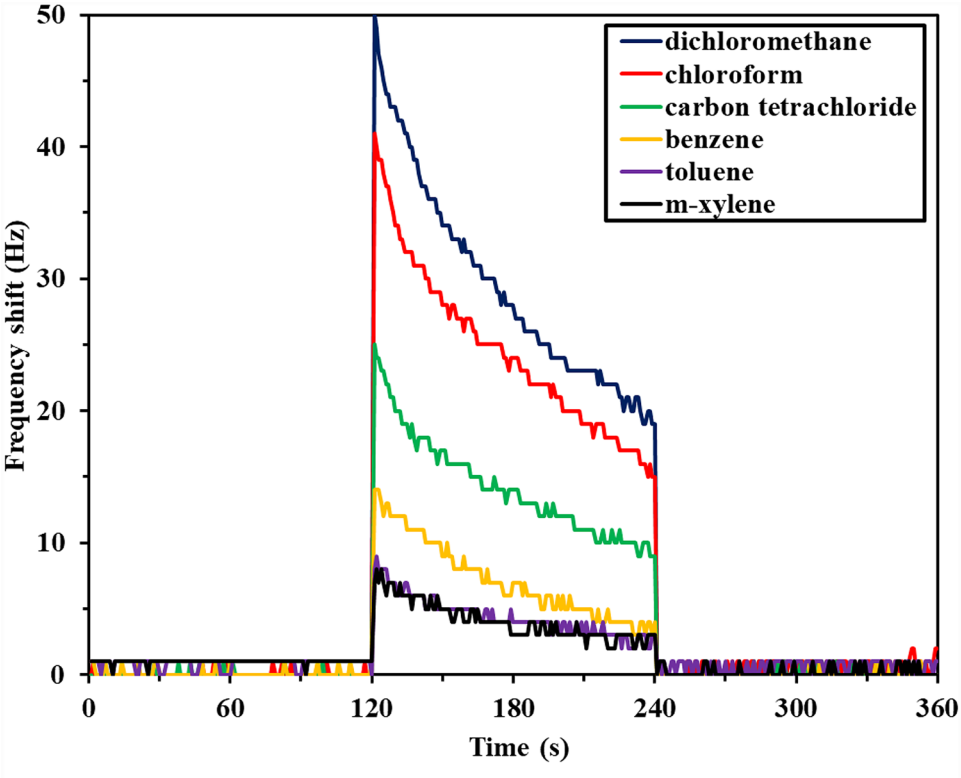

Fig. 4 The QCM kinetic results of graphene-coated QCM sensor for different VOCs

Table 1 The physical properties of VOCs

Organic vapors	Molar volume (cm^3 mol^{-1})	Vapor pressure (kPa, 20 ℃)
Dichloromethane	64.10	46.5
Chloroform	80.70	21
Carbon tetrachloride	97.10	12
Benzene	86.36	9.95
Toluene	107.10	2.91
m-xylene	122.00	0.8

Table 1 outlines the physical properties of vapors, highlighting dichloromethane as having the highest vapor pressure and the lowest molar volume. The observed increase in Δf values correlates with the upward trend in vapor pressure and the downward trend in molar volume. This observation suggests that the elevated vapor pressure and reduced molar volume contribute to an increased number of dichloromethane molecules. Consequently, stronger interactions with the sensing material may occur, leading to enhanced adsorption of dichloromethane molecules [56]. Also, the sensor's sensitivity to carbon tetrachloride, even though it is a nonpolar molecule, can be ascribed to its elevated vapor pressure.

Figure 5 presents transient response curves for the graphene-coated QCM sensor exposed to dichloromethane vapors at fixed (saturated) and increasing concentrations, evaluating both the reproducibility and reversibility of the sensor. A progressive increase in frequency variation (Δf) is observed with escalating vapor concentration, indicating good reproducibility. The sensor can recover to its initial state, demonstrating reliable performance in dichloromethane detection across a wide concentration range. The inset in the same figure displays transient measurement, with the saturated concentration of dichloromethane vapor, where reciprocal cycles, involving the application of the same concentration, demonstrate consistent and reversible Δf changes.

For SPR kinetic measurements, we adhered to the same testing protocol as in QCM measurements. The VOCs of interest were introduced into the dedicated gas cell for a 2-min injection period, followed by a 2-min recovery phase with the introduction of fresh air. During exposure to organic vapor, the change in reflected light intensity was recorded as a function of time.

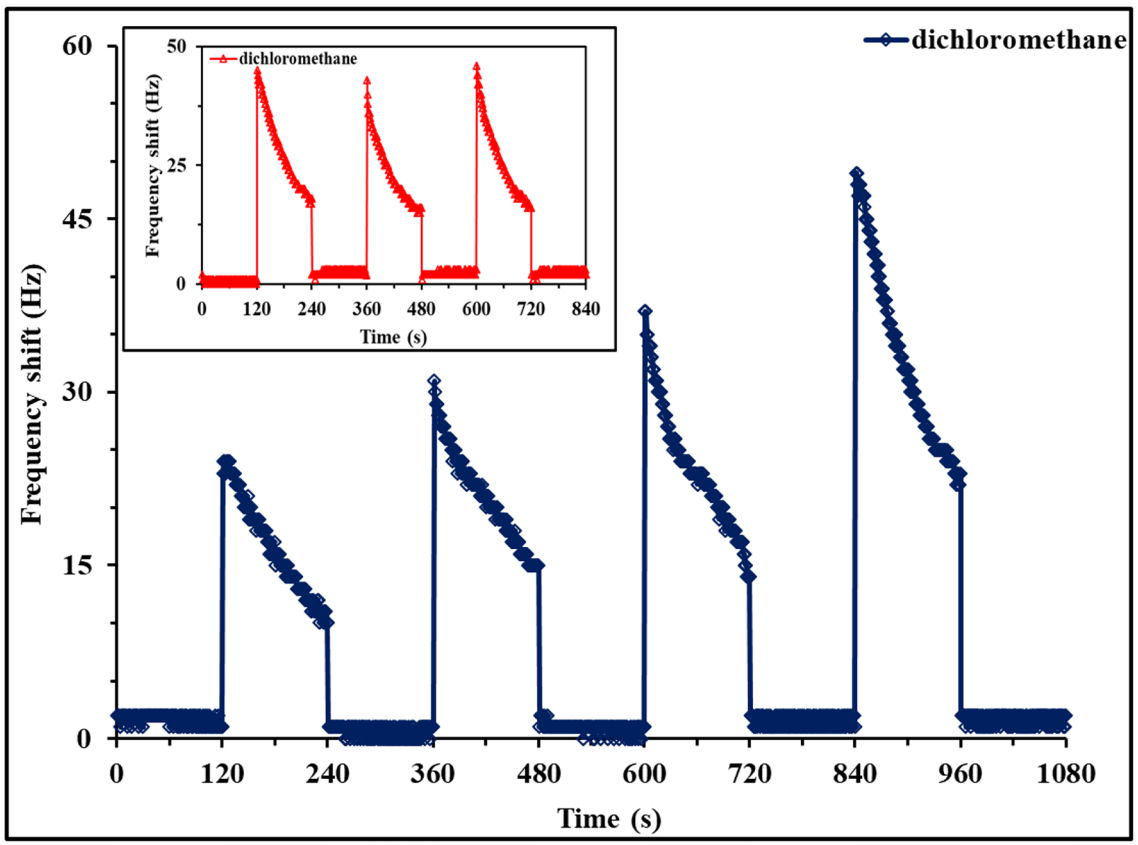

Fig. 5 The frequency shift of the graphene-coated QCM sensor over time in response to dichloromethane vapors at concentrations of 25%, 50%, 75%, and 100%. In the inset, the transient response curve of the sensor to the saturated concentration of dichloromethane showing repeatability

The responses of the graphene SPR sensor to saturated concentrations of identical vapors are illustrated in Fig. 6. Consistently, the same sensitivity order obtained in QCM measurements is observed, with dichloromethane eliciting the highest response. Notably, a discernible difference is observed—the initial peak upon the instant introduction of the vapor decays faster in the case of the SPR sensor compared to the QCM sensor.

Figure 7 shows transient measurements of the graphene-coated SPR sensor as the concentrations of dichloromethane increased. In this figure, the reflected light intensity values increase with the rising concentration of vapor exposure for each successive cycles. To confirm the reproducibility of the graphene-coated SPR optical sensor response (the inset in Fig. 7), the same concentration-based measurement was repeated with other VOCs, and the sensor consistently exhibited the same trend.

3.2 Sensitivity and LOD calculations

The limit of detection (LOD) is a critical parameter in sensor applications. The LOD values of graphene-coated SPR sensor were calculated by analyzing the standard deviation and sensitivity. The LOD is defined by the following equation [57]:

$$LOD = \frac{3\sigma}{S}, \tag{1}$$

where σ is the standard deviation (0.001) and S is the sensitivity. The sensitivity of the graphene-coated SPR sensor was determined by analyzing the slope of the calibration curve depicted in Fig. 8. This curve represents SPR response in relation to the concentration of dichloromethane vapor. The data indicate a strong linear correlation coefficient (R^2) of 0.9747 between the sensor response and the dichloromethane vapor concentration. The vapor concentration is calculated as

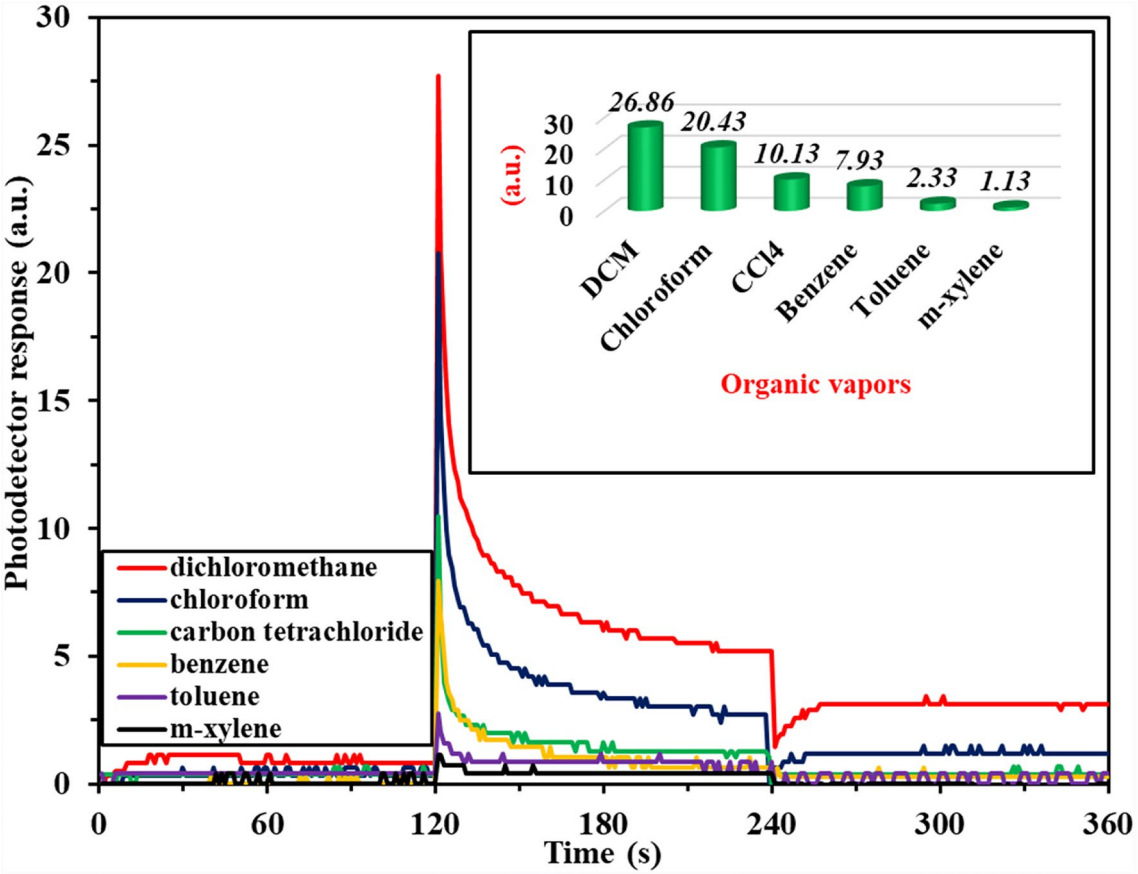

Fig. 6 The SPR kinetic results of graphene-coated SPR sensor for different VOCs

$$c = \frac{24.055\rho V}{MV_0} x10^6, \quad (2)$$

where ρ is the density of dichloromethane vapor, V is the injected vapor volume into the gas cell, M is the molecular weight of the vapor, and V_0 is the volume of the gas cell. In a similar manner, the sensitivity of the graphene-coated SPR sensor, for five other VOCs, was calculated. The results are presented in Table 2.

In Fig. 8, the rate of response is determined using the normalized response value expressed as a percentage. The variation in optical response, specifically the intensity of reflected light, is normalized using the equation:

$$NormalizedResponse\ (\%) = (\Delta I/I_0)x100, \quad (3)$$

where ΔI is the difference between the reflected light intensity (I) at any given time and the initial reflected light intensity (I_0) at the inception of the response ($t = 0$). The initial intensity serves as a baseline for this calculation.

The sensitivities of the graphene-coated SPR sensor toward VOCs were determined by analyzing the slopes of the calibration curves. The LOD values for each VOC were calculated using Eq. 1 and are given in Table 2. The lowest LOD value among aliphatic hydrocarbons is observed for dichloromethane, while the lowest LOD value among aromatic hydrocarbons is observed for benzene vapor. Among the six different gases tested in this study, dichloromethane had the lowest LOD value. The LOD for the graphene-coated SPR sensor ranged from 10.62 to 109.48 ppm and the sensitivity ranged from 0.027×10^{-3} to 0.294×10^{-3} ppm^{-1}.

Another crucial aspect in gas sensors is the assessment of response and recovery time. The response time, representing the duration for the sensor to achieve 90% of its final response, and the recovery time, indicating the time for the sensor to return to 90% recovery, are key parameters. These metrics are vital for a gas sensor's performance, underlining the need for a quick and efficient response to the target

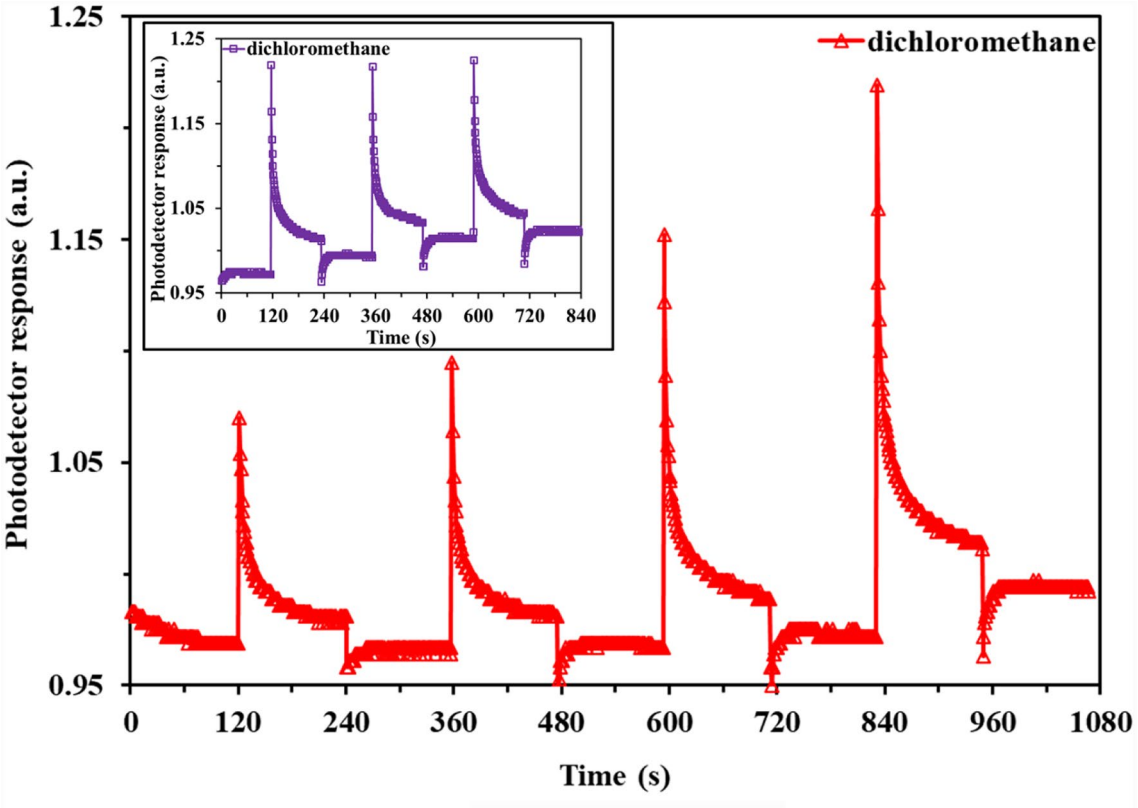

Fig. 7 Continuous monitoring of a graphene-coated SPR sensor in response to incrementally rising dichloromethane concentrations

gas. For the tested VOCs, the response and recovery times of the graphene-coated SPR sensor were found to be less than 3 sec.

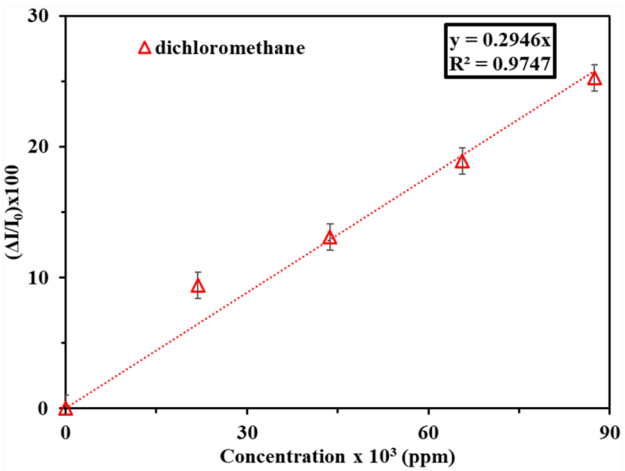

Fig. 8 Calibration curve of the graphene-coated SPR sensor to different concentrations of dichloromethane vapor

4 Conclusions

Two distinct sensing approaches, QCM and SPR, were employed to extensively investigate the sensing capabilities of CVD graphene against a variety of VOC molecules. Sensor devices were specifically designed for each transducing mechanism, incorporating CVD graphene as the sensing element. The graphene sensors exhibited consistent and reproducible responses when exposed to various concentrations of the tested VOCs.

Notably, both sensors exhibited the highest sensitivity to dichloromethane among the tested VOC molecules. The sensitivity of the graphene-coated SPR sensor for dichloromethane is 0.294×10^{-3} ppm^{-1}, with an LOD value of 10.62 ppm. Additionally, the SPR sensor exhibited remarkably low response and recovery times, both being less than 3 sec.

In summary, our investigation unveils the excellent performance of CVD graphene in VOC sensing, highlighting its potential for precise and reliable gas sensing applications. Furthermore, taking into account graphene's remarkable electronic properties, such as

Table 2 The sensitivity, LOD, response time, and recovery time values for graphene-coated SPR sensor to VOCs

	Sensitivity ($\times 10^{-3}$ ppm^{-1})	LOD (ppm)	Response time (s)	Recovery time (s)
Dichloromethane	0.294	10.62	1.5	2
Chloroform	0.263	11.38	1.5	2
Carbon tetrachloride	0.089	33.37	2	2.5
Benzene	0.150	19.92	2	2
Toluene	0.054	55.35	2.5	2.5
m-Xylene	0.027	109.48	3	3

high mobility and an exceptional signal-to-noise ratio, we anticipate that graphene holds significant promise as a sensing electrode in electrochemical platforms for VOC detection.

Author contributions

HS and YA contributed toward conceptualization, methodology, formal analysis, data curation, investigation, visualization, writing, and review. IC and RC contributed toward supervision, Formal analysis, data curation, investigation, visualization, writing, and review.

Funding

Open access funding provided by the Scientific and Technological Research Council of Türkiye (TÜBİTAK). The authors have not disclosed any funding.

Data availability

Data sharing is not applicable to this article as no datasets were generated or analyzed during the current study.

Declarations

Conflict of interest The authors declare that they have no competing interests.

References

1. S.-K. Song, Z.-H. Shon, Y.-H. Kang, K.-H. Kim, S.-B. Han, M. Kang, J.-H. Bang, I. Oh, Environ. Pollut. **247**, 763 (2019)
2. V. Soni, P. Singh, V. Shree, V. Goel, *Air Pollution and Control* (Springer, Singapore, 2018), p.119
3. Z.F. Zhang, X. Zhang, X. Zhang, L.Y. Liu, Y.F. Li, W. Sun, Chemosphere **250**, 126324 (2020)
4. World Health Organization, *WHO Guidelines for Indoor Air Quality: Selected Pollutants* (World Health Organization, Geneva, 2010)
5. J.P. Sá, M.C.M. Alvim-Ferraz, F.G. Martins, S.I.V. Sousa, Environ. Technol. Innov. **28**, 102551 (2022)
6. W. Yu, X. Shen, Z. Yao, X. Cao, X. Hao, X. Li, B. Wu, H. Zhang, S. Wang, Q. Zhou, Sci. Total. Environ. **914**, 169844 (2024)
7. C. Xing, C. Liu, J. Lin, W. Tan, T. Liu, J. Hazard. Mater. **461**, 132573 (2024)
8. B. Han, T.H. Rupam, A. Chakraborty, B.B. Saha, Renew. Sustain. Energy Rev. **196**, 114365 (2024)

9. M. Lueno, H. Dobrowolny, D. Gescher, L. Gbaoui, G. Meyer-Lotz, C. Hoeschen, T. Frodl, Front. Psychiatry **13**, 819607 (2022)
10. J.E. Belizário, J. Faintuch, M.G. Malpartida, Front. Cell. Infect. Microbiol. **10**, 564194 (2021)
11. J. Song, R. Li, R. Yu, Q. Zhu, C. Li, W. He, J. Liu, Microchem. J. **199**, 110051 (2024)
12. E. Bonah, X. Huang, J.H. Aheto, R. Osae, J. Food Sci. Technol. **57**, 1977 (2020)
13. X. Li, J. Zhu, C. Li, H. Ye, Z. Wang, X. Wu, B. Xu, Molecules **23**, 3286 (2018)
14. Y. Zhang, L. Guo, Z. Qiu, Y. Lv, G. Chen, E. Li, J. Clin. Lab. Anal. **34**, e23526 (2020)
15. C. Wei-Ni, Y. Zi-Cheng, C. Shen-Hui, Z. Ying-Tong, X. Guo-Bin, D. Dan-Dan, S. Xin, Z. Peng, W. Man-Man, H. Bin, Chin. J. Anal. Chem. **50**, 445 (2022)
16. S. Acharyya, S. Nag, S. Kimbahune, A. Ghose, A. Pal, P.K. Guha, ACS Sens. **6**, 2218 (2021)
17. R.A.B. John, A.R. Kumar, Inorg. Chem. Commun. **133**, 108893 (2021)
18. P. Kumar, K.H. Kim, P.K. Mehta, L. Ge, G. Lisak, Crit. Rev. Environ. Sci. Technol. **49**, 2016 (2019)
19. Z. Khatoon, H. Fouad, O.Y. Alothman, M. Hashem, Z.A. Ansari, S.A. Ansari, ACS Omega **5**, 27645 (2020)
20. G.C. Rezende, S. Le Calvé, J.J. Brandner, D. Newport, Sens. Actuators B. **287**, 86 (2019)
21. M. Wei-Hao Li, A. Ghosh, A. Venkatasubramanian, R. Sharma, X. Huang, X. Fan, ACS Sens. **6**, 2348 (2021)
22. R.D. Prasad, R.S. Prasad, Y.I. Shaikh, S.R. Prasad, M.N. Padvi, P.D. Sarvalkar, S. Saxena, V.S. Shaikh, G.M. Nazeruddin, S. Shaikh, A.B. Kanwade, N. Charmode, A.K. Vaidya, O.P. Shrivastav, C.B. Desai, P.D. Patil, ES Mater. Manuf. **23**, 1084 (2024)
23. E. Fernandez, P.G. Saiz, N. Peřinka, S. Wuttke, R. Fernández de Luis, Adv. Funct. Mater. **31**, 2010703 (2021)
24. X. Huang, Y. Li, E. Witherspoon, R. He, G. Petruncio, M. Paige, M. Li, T. Liu, K. Amine, Z. Wang, Q. Li, P. Dong, ACS Sens. **8**, 3389 (2023)
25. F. Kus, C. Altinkok, E. Zayim, S. Erdemir, C. Tasaltin, I. Gurol, Sens. Actuators B **330**, 129402 (2021)
26. A.K. Pathak, C. Viphavakit, Sens. Actuators A **338**, 113455 (2022)
27. X. Qu, Y. Hu, C. Xu, Y. Li, L. Zhang, Q. Huang, S.S. Moshirian-Farahi, J. Zhang, X. Xu, M. Liao, Y. Fu, Chem. Eng. J. **485**, 149804 (2024)
28. C.K. McGinn, Z.A. Lamport, I. Kymissis, ACS Sens. **5**, 1514 (2020)
29. F. Yin, W. Yue, Y. Li, S. Gao, C. Zhang, H. Kan, H. Niu, W. Wang, Y. Guo, Carbon **180**, 274 (2021)
30. M. Khatib, H. Haick, ACS Nano **16**, 7080 (2022)
31. M. Tomić, M. Šetka, L. Vojkůvka, S. Vallejos, Nanomaterials **11**, 552 (2021)
32. S. Shi, W. Xu, B. Zhou, S. Qin, X. Liu, H. Li, Adv. Compos. Hybrid Mater. **6**(1), 168 (2023)
33. A.C. Ferrari, F. Bonaccorso, V. Fal'ko, K.S. Novoselov, S. Roche, P. Bøggild, S. Borini, F.H.L. Koppens, V. Palermo, N. Pugno, J.A. Garrido, R. Sordan, A. Bianco, L. Ballerini, M. Prato, E. Lidorikis, J. Kivioja, C. Marinelli, T. Ryhänen, A. Morpurgo, J.N. Coleman, V. Nicolosi, L. Colombo, A. Fert, M. Garcia-Hernandez, A. Bachtold, G.F. Schneider, F. Guinea, C. Dekker, M. Barbone, Z. Sun, C. Galiotis, A.N. Grigorenko, G. Konstantatos, A. Kis, M. Katsnelson, L. Vandersypen, A. Loiseau, V. Morandi, D. Neumaier, E. Treossi, V. Pellegrini, M. Polini, A. Tredicucci, G.M. Williams, B. Hee Hong, J.H. Ahn, J. Min Kim, H. Zirath, B.J. van Wees, H. van der Zant, L. Occhipinti, A. Di Matteo, I.A. Kinloch, T. Seyller, E. Quesnel, X. Feng, K. Teo, N. Rupesinghe, P. Hakonen, S.R.T. Neil, Q. Tannock, T. Löfwander, J. Kinaret, Nanoscale **7**, 4598 (2015)
34. K.S. Novoselov, A.K. Geim, S.V. Morozov, D. Jiang, Y. Zhang, S.V. Dubonos, I.V. Grigorieva, A.A. Firsov, Science **306**, 666 (2004)
35. E.W. Hill, A. Vijayaragahvan, K. Novoselov, IEEE Sens. J. **11**, 3161 (2011)
36. J. Miao, T. Fan, Carbon **202**, 495 (2023)
37. P. Jain, R.S. Rajput, S. Kumar, A. Sharma, A. Jain, B.J. Bora, P. Sharma, R. Kumar, M. Shahid, A.A. Rajhi, M. Alsubih, M.A. Shah, A. Bhowmik, ACS Omega **9**, 12403 (2023)
38. S.R. Karanjikar, A.S. Sena, P. Manekar, S. Mudagi, A.S. Juneja, Mater. Today Proc. **50**, 2007 (2022)
39. Y. Jia, J. Zhang, D. Kong, C. Zhang, D. Han, J. Han, Y. Tao, W. Lv, Q.H. Yang, Adv. Funct. Mater. **32**, 2204272 (2022)
40. D.J. Buckley, N.C.G. Black, E.G. Castanon, C. Melios, M. Hardman, O. Kazakova, 2D Mater. **7**, 032002 (2020)
41. F. Fauzi, A. Rianjanu, I. Santoso, K. Triyana, Sens. Actuators A **330**, 112837 (2021)
42. F. Schedin, A.K. Geim, S.V. Morozov, E.W. Hill, P. Blake, M.I. Katsnelson, K.S. Novoselov, Nat. Mater. **6**, 652 (2007)
43. F. Moriggi, V. Barbera, M. Galimberti, G. Raffaini, Molecules **28**, 7633 (2023)
44. S.S. Dindorkar, N. Sinha, A. Yadav, Solid State Commun. **359**, 115021 (2023)
45. H. Wu, N. Yu, W. Liu, IEEE Sens. J. **24**, 7490 (2024)
46. W. Ju, S. Lee, Nanomaterials **13**, 243 (2023)
47. N. Alzate-Carvajal, J. Park, I. Bargaoui, R. Rautela, Z.J. Comeau, L. Scarfe, J.M. Ménard, S.B. Darling, B.H. Lessard, A. Luican-Mayer, ACS Appl. Electron. Mater. **5**, 1514 (2023)

48. A.C. Ferrari, J.C. Meyer, V. Scardaci, C. Casiraghi, M. Lazzeri, F. Mauri, S. Piscanec, D. Jiang, K.S. Novoselov, S. Roth, A.K. Geim, Phys. Rev. Lett. **97**, 187401 (2006)
49. G. Sauerbrey, Z. Phys. **155**, 206 (1959)
50. J. Homola, M. Piliarik, *Surface Plasmon Resonance (SPR) Sensors* (Springer, New York, 2006)
51. S.A. Maier, *Plasmonics: Fundamentals and Applications* (Springer, New York, 2007)
52. B. Kumar, K. Min, M. Bashirzadeh, A.B. Farimani, M.-H. Bae, D. Estrada, Y.D. Kim, P. Yasaei, Y.D. Park, E. Pop, N.R. Aluru, A. Salehi-Khojin, Nano Lett. **13**, 1962 (2013)
53. U.V. Patil, A.S. Pawbake, L.G.B. Machuno, R.V. Gelamo, S.R. Jadkar, C.S. Rout, D.J. Late, RSC Adv. **6**, 48843 (2016)
54. V. Van Quang, V.N. Hung, L.A. Tuan, V.N. Phan, T.Q. Huy, N. Van Quy, Thin Solid Films **568**, 6 (2014)
55. O. Leenaerts, B. Partoens, F.M. Peeters, Phys Rev B **77**, 125416 (2008)
56. K. Büyükkabasakal, S. Celik Acikbas, A. Deniz, Y. Acikbas, R. Capan, M. Erdogan, IEEE Sens. J. **19**, 9097 (2019)
57. Y. Acikbas, Res. Eng. Struct. Mat. (2023). https://doi.org/10.17515/resm2023.57ma1027rs